Energy Technology
Generation, Conversion, Storage, Distribution
www.entechnol.de

Correlation of Health Indicators on Lithium-Ion Batteries

Philipp Dechent, Elias Barbers, Alexander Epp, Dominik Jöst, Weihan Li, Dirk Uwe Sauer, and Susanne Lehner*

Herein, a detailed correlation index of health indicators for lithium-ion batteries is presented. Identifying potential correlations of health indicators is of high importance with regard to the cell selection process and to minimize the occurring cell-to-cell spread within the lifetime. Health indicators that are taken into account are among others impedance measurements of different pulse lengths, capacity values at different discharge procedures and checkups, weight, and initial voltage. Herein, the work is based on four different aging datasets covering variations in cell chemistry (NMC, LFP, NCA), cell type (round, prismatic), as well as the size and designated application (consumer, automotive). A publicly available dataset is included to allow for an easy reproduction of the results.

1. Introduction

Longevity of batteries is beneficial and can reduce the total cost of ownership, but it becomes essential for large automotive and stationary-storage systems. Especially in industrial-scale stationary applications, design lifetimes have to be in the range of 10–15 years.[1] The same applies to the emerging market of marine hybridization. This is compounded by the fact that large stationary and marine storage systems in the MWh range consist of thousands of cells, with the racks of an array connected directly in parallel on a common DC link. These DC links typically have a high nominal voltage in excess of 800 V. To avoid large imbalances in the system, three conditions must be met. While uniform operating conditions must be ensured at the system level, for example, through uniform temperature distribution, the other two conditions must be met at the cell level or in the cell selection process. First, high-quality cells must be used, resulting in a minimum spread of cell-to-cell variation over the lifetime of the system.[2] Secondly, during the cell selection process, measures must be found to grade the cells and exclude cells with potentially deviating behavior from the good-to-use cells.[3]

In automotive applications, system size is currently limited to a comparatively small size below 100 kWh.[4] However, as they are mass-produced and cost savings potential should be addressed at both the cell and system level, direct cell-to-pack architectures such as the BYD Auto Ltd. Blade are being considered.[5] This results in a highly individual cell capacity. The disadvantage is that there is no smoothing behavior of a parallel connection at the cell level. Finally, large-scale systems tend to follow automotive trends to achieve economies of scale. Therefore, increasing cell capacity can be expected in these applications as well.

However, there are many factors that can lead to increased inhomogeneities in cell capacity and/or impedance within a set of battery cells. The most immanent ones, which are addressed in various aging analyses, are the respective operating conditions such as charge and discharge rates, depth of discharge (DoD), and mean state of charge (MOS), temperatures, as well as the state of charge during idle periods. In addition, system integration can have a significant impact. Examples include uneven and/or defective cell contacts, an improperly designed cooling system or other external thermal influences, and cell bracing.[6,7] Finally, there are also production-related effects that result in divergent aging behavior, especially when mismatched cells are used in the battery pack. These inhomogeneities can be attributed to manufacturing tolerances[8,9] and the formation process, as well as varying conditions during shipping and storage. Strictly speaking, the latter is a normal calendar aging under different conditions. However, since it occurs before integration into modules, it must be considered as an initial deviation in the new state.

In this study, we explore the correlation of different health indicators and show the value to inform the design of experiment with avoiding time-consuming tests within a checkup procedure when they do not give much more information. In addition, "free" health indicators without additional testing cost like the resistance of a reoccurring voltage drop should be used to increase the information from a given test or cell selection process.

P. Dechent, E. Barbers, A. Epp, D. Jöst, W. Li, D. U. Sauer
Chair for Electrochemical Energy Conversion and Storage Systems
RWTH Aachen University
52062 Aachen, Germany
E-mail: philipp.dechent@isea.rwth-aachen.de

P. Dechent, E. Barbers, A. Epp, D. Jöst, W. Li, D. U. Sauer
Jülich Aachen Research Alliance
JARA-Energy
52425 Jülich, Germany

E. Barbers, D. U. Sauer
Helmholtz Institute Münster (HI MS)
IEK-12
Forschungszentrum Jülich
52066 Aachen, Germany

S. Lehner
Technology Development
MAN Energy Solutions SE
86153 Augsburg, Germany

The ORCID identification number(s) for the author(s) of this article can be found under https://doi.org/10.1002/ente.202201398.

DOI: 10.1002/ente.202201398

2. State of the Art

The demand for a decent understanding of lithium-ion battery aging at the cell level and its correlated cell-to-cell variation is a highly addressed topic in battery research. In addition, multiple health indicators can be used as features for machine-learning applications[10] or a vector state representation for overall battery health.[11] In the following, an introduction to state of the art shall be given. As it focuses mostly on either the understanding of the aging processes itself and their parameter dependency or the cell-to-cell variations, the state of the art of the two focus areas shall be presented individually, starting with the aging experiments.

2.1. Aging Experiments and Aging Evaluation

Lithium-ion batteries are not operating in a thermodynamic-stable region. Thus, they must only be used in a chemistry-dependent operating window to limit degradation due to side reactions that take place both during usage as well as during storage. Experiments are carried out individually for cyclic and calendar aging.[12] Yet, at that point, it needs to be noted that the latter is always superimposed and, therefore, needs to be accounted for also in all cyclic aging experiments.[13] Accelerating factors that are extensively studied are temperature, state of charge (SoC), DoD, and C-rate. Yet, depending on cell shape, further influencing factors such as bracing must not be neglected. The main corresponding degradation mechanisms are electrolyte decomposition, growth of the solid electrolyte interface (SEI), solvent co-intercalation, content loss of active material, decomposition of binder, current collector corrosion, and cell internal short circuits. An overview of these mechanisms can be found, for example, in refs. [14,15]. The degree of impact of the individual mechanisms depends on the severity of the different operating factors that are known to accelerate aging, for example, operation at low temperatures will specifically enhance SEI growth, whereas overcharge is more associated with a solvent co-intercalation.

Moreover, to draw conclusions from single-cell aging in a laboratory environment on the aging on the system level, one has to take into account various topology-related effects. This is mainly due to the fact that uneven boundary conditions have to be considered but also—as explained in the next section—by the distribution of the cell performance itself. With regard to the topology, it can be distinguished by external factors that have an influence on the individual cells, such as, for example, temperature spread. Especially in large systems, a spread of around 3–5 °C has to be considered realistic under operation, yet also higher spreads are reported. Also, cell bracing on module level will add to a certain difference. The same is true for different current collectors at module interfaces.

These boundary factors can further enhance the effect of the electrical topology. While a parallel connection on the cell level might lead to a natural minimization of cell-to-cell variations, especially a parallel interconnection of complete systems comes along with a high potential impact of circulating currents. An example of that is large stationary-storage systems with a nominal voltage level of around 800 V on rack level that are usually directly connected in parallel on a DC bus bar. With several racks being connected to the common bus bar, a slight difference in the individual racks can lead to a high imbalance in the overall load, especially in the operating boundaries. Hence, it can have an aging effect that one must not neglect. Moreover, the SoC difference that allows for interconnection of the racks needs to be kept in a narrow window to limit the effect.

2.2. Cell-To-Cell Variation Analysis

The cell-to-cell variations, already mentioned in the previous section, are a widely known and investigated cell performance and, ultimately, safety-altering issue. These variations are not only caused by the always, to some extent, differing aging conditions on the system level but also by disparities in the materials used and their chemical composition, the processing and formation as well as the cell formats and connectors. There are diverse studies like, for example ref. [9], with varying amounts of cells analyzing this inhomogeneity, often also using complex mapping techniques.[16] The found spread on reaching end-of-life conditions is tremendous with, for example, more than 350 full cycle equivalents (FCEs) at an average lifetime of 1100 FCE in the analysis of Baumhöfer et al.[9] The results are backed by further studies such as, for example ref. [17], which found an even higher imbalance. The analysis of Schuster et al.[18] showed that most of the far outliers age faster than the average.

Yet, for scaling it to the system level and also using it within the online management tools, more investigations with regard to reproducibility and statistical representation are still required. Especially for large-scale applications that are more and more to come, especially in stationary applications, this is an urgent requirement to forecast performance and durability even if the aging spread can be further minimized by an optimized production process. For more details on the deviation causes as well as an overview of carried out studies, the authors refer to a recent review by Beck et al.[16].

3. Dataset Description

The following list introduces the testsets which are analyzed in this paper. It gives an overview of the main testset boundaries. Moreover, it states the identifier used later on to distinguish between the different testsets. The testset of Preger–2020 is available open access and can be found at batteryarchive.org for all considered cell types. 1) Baumhöfer–2014[9] consists of 48 Sanyo/Panasonic UR18650E NMC/carbon 1.85 Ah cells in a cycle aging test, each under the same operating conditions. The testset is used in the analysis of initial cell parameters at delivery. 2) Preger–2020,[19] A123 APR18650M1A, 1.1 Ah, 18 650; Panasonic NCR18650B, 3.2 Ah, 18 650; LG Chem 18650HG2, 3 Ah, 18 650. The testset is used to illustrate the comparison of chemistries. 3) Schöneberger–2019,[20] LiTec HEI40 40 Ah, automotive large-scale pouch cells. The testset is used in the analysis of calendar and cyclic test conditions. 4) Willenberg–2021,[21] Samsung INR18650-35 E, NCA/graphite cell with nominal capacity of 3.4 Ah cylindrical 18 650 type. The testset is used in the analysis of initial cell parameters at delivery.

A comprehensive overview of the cell parameters of the individual testsets according to the respective datasheets is provided in **Table 1**. The three different cells used in the openly available dataset by Preger–2020 are indicated by the numbers one to three—namely 1) Lithium iron phosphate (LFP), 2) Lithium nickel cobalt

Table 1. Analyzed cells of the individual testsets.

	Baumhöfer–2014	Preger–2014 (1,2,3)	Schöneberger–2019	Willenberg–2021
Manufacturer	Sanyo/Panasonic	A123 (1) Panasonic (2) LG Chem (3)	LiTec	Samsung
Cell name	UR18650E	APR18650M1A (1) NCR18650B (2) 18650HG2 (3)	HEI40	INR18650–35 E
Number of aged cells	48	28 (1) 22 (2) 24 (3)	13 cycle 30 calendar	183
Cell type	18 650	18 650 (1,2,3)	Pouch	18 650
Cathode material	NMC	LFP (1) NCA (2) NMC (3)	NMC	NCA
Nominal capacity [Ah]	1.85	1.1 (1) 3.2 (2) 3 (3)	40	3.35
Nominal voltage [V]	3.6	3.3 (1) 3.6 (2, 3)	3.6	3.6
Min. voltage [V]	2.5	2 (1, 3) 2,5 (2)	3	2.65
Max. voltage [V]	4.2	3.6 (1) 4.2 (2, 3)	4.2	4.2
Max. charge current [A]	2.05	4 (1) 1.625 (2) 6 (3)	80	2
Max. discharge current [A]	6.15	30 (1) 6 (2) 20 (3)	120	8
Mass [g]	45.5	39 (1) 48.5 (2) 47 (3)	1200	50

Table 2. Explanation of the health indicators.

Indicator	Description
Initial capacity	First measured discharge capacity
Second capacity	Measured discharge capacity at first checkup
Weight	Measured cell weight
Initial voltage	Cell voltage at delivery
1 kHz impedance	1 kHz impedance measured at delivery
Impedance	Impedance determined using different pulse currents (in C-rates), duration (in seconds) and observed cell SoC (in %). Example ResCHA1C2sec30 is a charge pulse resistance with a current of 1C after 2 s at a SoC of 30%.
Capacity–DCH	Measured discharge capacity until lower voltage limit is reached
Capacity–CHA	Measured capacity of constant current phase (CC) until the upper voltage limit is reached
Capacity–CHA–CV	Measured capacity of constant voltage phase (CV) until the current has fallen below a predefined limit
Mean temp.	The mean cell temperature within the test

Table 3. Analyzed health indicators of the individual testsets.

Indicator	Baumhöfer–2014	Preger–2014	Schöneberger–2019	Willenberg–2021
Initial capacity	x	–	–	x
Second capacity	x	–	–	x
Weight	–	–	–	x
Initial voltage	–	–	–	x
1 kHz impedance	–	–	–	x
Impedance	x	x	x	–
Capacity–DCH	–	x	x	–
Capacity–CHA	x	x	x	–
Capacity–CHA–CV	–	x	–	–
Mean temp.	x	x	–	–

aluminium oxides (NCA), 3) and Lithium nickel manganese cobalt oxides (NMC). All testsets in addition to the one of Schöneberger–2019 feature 18 650 cells and, thus, consumer cells that are respectively publicly available. The C-rate in the charge direction is in the range of 0.6–3.6 and in the discharge direction in the range of 1.9–27.2. Hence, cells of a substantially differing power capability and, therefore, cell structure were analyzed.

As already indicated in the list of testsets, not every analysis is presented for all testsets. Therefore, an overview of investigated health indicators can be found in **Table 2** and the corresponding allocation to the investigations of each testset is shown in **Table 3**.

4. Description of the Plots Shown in This Paper

A multi-plot with an even amount of subplots aligned in *x*- and *y*-direction, as shown in **Figure 1**, is used as the main visual element to analyze the correlation of the health indicators. Its content shall be briefly introduced. The health indicators, such as, for example, initial capacity and cell weight, are pairwise combined by using each health indicator once as a column identifier and once as a row identifier.

As the *n*th position in row and column has the same identifier, the identity relationship is shown on the diagonal from upper left to lower right. It is depicted as a kernel density estimation (KDE) which smooths the observed values by a Gaussian kernel to a continuous density estimation rather than depicting, for example, the values binned in histograms. The general shape of the KDE allows us to identify the individual distribution function of a parameter visually and by a goodness-of-fit test. The maxima indicate the most likely values. The *y*-axis has no meaning for those plots, the values of the KDE add up to 100% and depict the relative spread of values. Care must be taken when comparing kernel density estimates between two data sets, as the choice

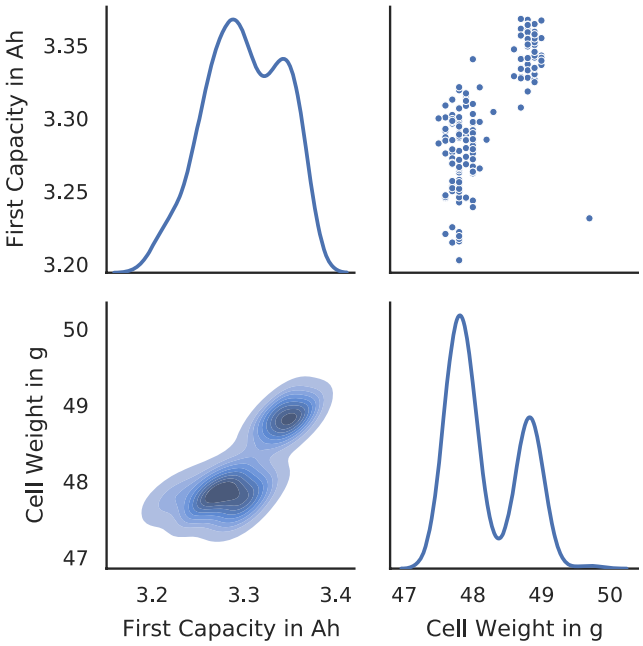

Figure 1. Explanation of the main depicting scheme of this work. The used multi-plot consists of the kernel density estimation (KDE) plots on the diagonal from upper left to lower right, the scatter plots in the upper triangle, and the bivariate KDE contour plots in the lower triangle.

of kernel function and bandwidth can greatly affect the resulting estimate through the applied smoothing. In addition, KDEs are sensitive to outliers, making comparisons between datasets with different levels of outliers difficult.

In the upper triangle, the discrete measurement points are depicted in a scatter plot. Clusters and linear dependencies are visualized by the resulting point clouds. A drawback of scatter plots is that the various points can overlap and thus become invisible. This is valid, especially for large testsets with pronounced data pairs. All plots in this work are created with the python library seaborn.

In the lower triangle, the same combination of health indicators is analyzed but with a reversed x- to y-axis allocation. Instead of scattering, the bivariate KDE contour plot is drawn with each line indicating the region that contains the value pairs resulting in a density above the line's threshold. Hence, especially pronounced areas of a high density can be identified very easily by the plot and the steepness in the different directions around them.

5. Initial Parameters

5.1. Comparing Initial Parameters

Figure 2 shows the initial capacity and the capacity at the second checkup in Ah, the cell weight in g, the initial voltage before cycling in V, and a 1 kHz impedance in Ω measured upon arrival from Willenberg–2021. The 18 650 cylindrical cells from Samsung SA35E were bought in three batches in March 2018, November 2018, and November 2019, respectively. These batches are depicted in different colors within the scatter plot to distinguish between them—namely blue (first batch), orange (second batch), and green (third batch).

Batch one shows a higher variation with regard to the initial parameters in general and differs the most from the other two batches which were purchased at a later point in time. This might be an indication of changes in the production process, formation or materials used. Hence, it is important to analyze a cell behavior in detail to rely on cells of a common batch to avoid the risk of false correlations. The same relevance is obviously given in the pack design.

Cells from the first batch showed a lower initial capacity compared to the latter two. The cells showed a higher impedance while being, on average, around 1 g lighter, which is about 2% of the cell's weight given in the datasheet. Cells within the batches varied below 1 g, while in total, the lightest and heaviest cells differed at around 2 g. In the initial voltage at delivery, a batch dependence is also visible. This can be caused by material differences or differences in storage time since this can reduce the charge within the battery through calendar aging. Similar differences over the production cycle were reported by Schindler et al.[22]. The initial capacity ranges between 3.3 and 3.4 Ah, with bigger variances observed than other single datasets, for example, by Kuntz et al.[23] with a mean discharge capacity of 3.328 Ah and a standard deviation of 0.019 Ah. This can be attributed to a slightly bigger current of 0.3 C or batch dependence. Similar differences over the production cycle are reported, for example, by Schindler et al.[22]. Kuntz et al. also observed tighter tolerances within the cell weight with a standard variation of only 40 mg. The 1 khz impedance varied within the dataset from around 20–24 mΩ, with a strong batch dependence. This resistance is highly temperature sensitive, so it needs to be accounted for when checking at delivery and cell needs to be adjusted to the same temperature.

Figure 3 depicts the initial parameters for the Baumhöfer–2014 set. Here displayed are the initial capacity, the capacity of the second checkup, the capacity during the constant current charging phase, the mean temperature in Celsius during the checkup, and two discharge pulse resistance values at 1 C and 50% SoC at 2 and 10 s. For this evaluation, the 1 C capacity is used, so they are slightly varying from the values depicted in the capacity versus cycles plots in Baumhöfer et al.[9]

The first discharge capacity shows values between 1.76 and 1.79 Ah increasing to a spread of 1.70–1.75 Ah in the second checkup. There is a correlation visible between the first and second checkups, with higher first capacities also trending to higher second capacities. But some of the lowest values of the second capacity show comparably high first capacity values. So, the first capacity captures the general trend, but higher aging rates cannot be captured, resulting in differences in the second capacity. The capacity from the constant current charge shows no clear trend compared to the first or second capacity. A small temperature dependence can be seen between test temperature and resistance, with higher temperatures leading, in general, to lower resistance values as is expected. The mean temperature of the whole checkup ranges from 26.5 to 28.5 °C and the other values do not show an influence of temperature in the depicted range.

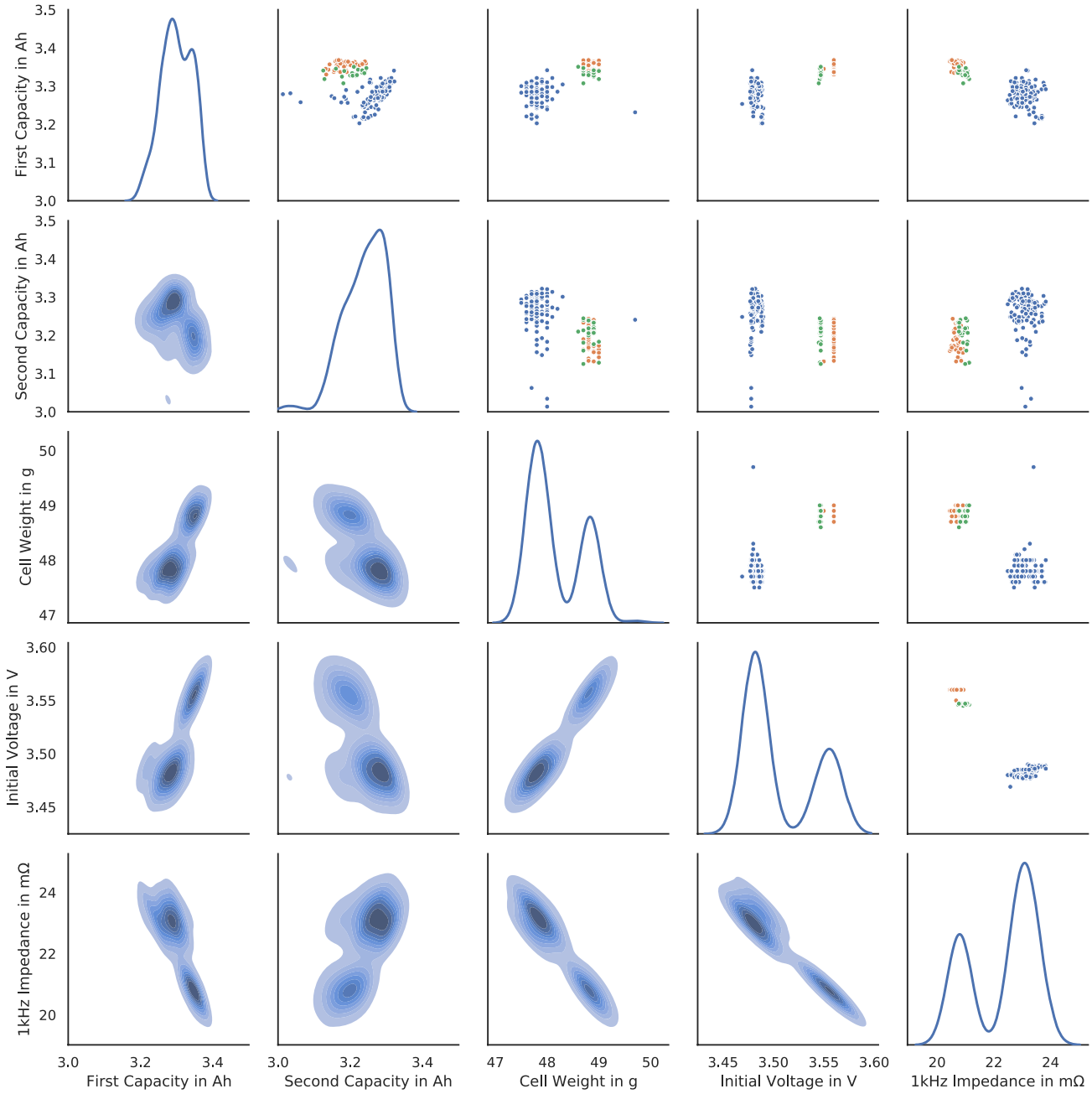

Figure 2. Correlation of the following initial parameters of the dataset Willenberg–2021: initial capacity, second capacity value, cell weight, initial voltage, and 1 kHz impedance. Capacities are determined within the checkup procedure, and weight, voltage, and impedance are recorded at delivery. Cells were bought in three batches, which can be distinguished by the following colors: blue (batch 1), orange (batch 2), and green (batch 3).

5.2. Pulse Resistance

The pulse resistance values of varying checkups shall be investigated more in detail using a heatmap. To illustrate its content, first, a subset of the values is depicted in **Figure 4**a. Here, three different pulse resistance values are shown, and all values over the whole lifetime of all cells correlated. The correlation coefficient for each pairing is given in the lower-left corner as part of the scatter plots. In the next step, Figure 4 shows the same correlation but as a heat map. Each resistance is shown once on the *x*-axis and on the *y*-axis, and the correlation coefficient for each pairing is given as a color code at the intersection and a legend at the side. A bright value depicts a good correlation between two pulse resistances, a dark value shows poor or no correlation.

The correlation in Figure 4 and **5** includes values from each checkup over the whole lifetime of all cells of the Baumhöfer–2014 dataset. The labels are named in the following way: Res

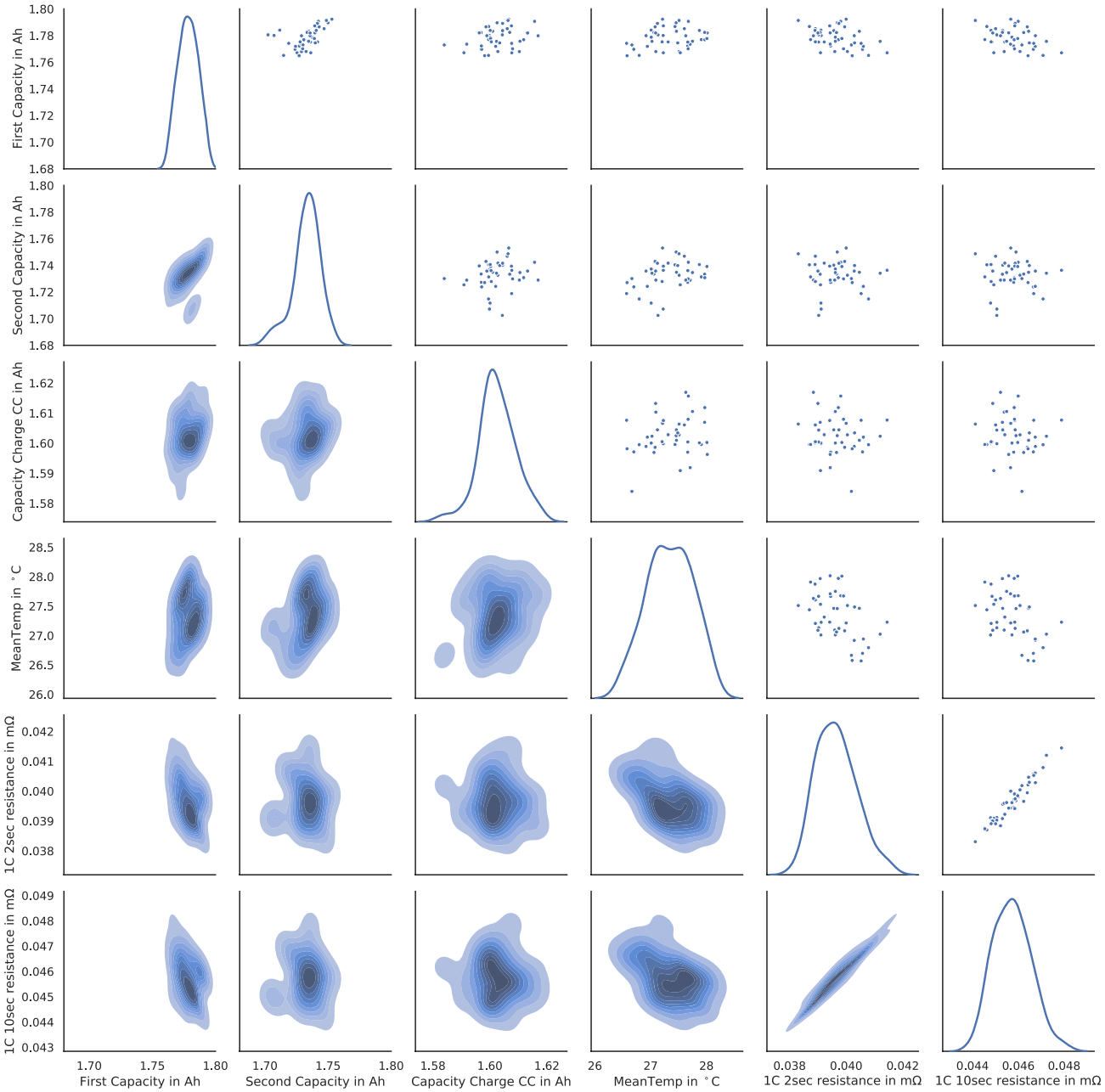

Figure 3. Correlation of the following initial parameters of dataset Baumhöfer et al.:[9] initial capacity, second capacity value, charge capacity during the constant current phase, mean temperature during the checkup and 2 and 10 s pulse resistances at 1 C, 50% state of charge (SoC). All values are determined within the checkup procedure.

is short for resistance, CHA for charge pulse and DCH for discharge pulse, next to the current as a C-rate, a leading zero indicates a fraction, so 025 indicates 0.25 C, afterward the pulse length either 2 or 10 s and last the SoC in percent. Concluding ResCHA1C2sec30 is a charge pulse resistance with a current of 1 C after 2 s at an SoC of 30%. Overall, the correlation of pulse resistances within this dataset is very high, with lowest values still above 0.98. Pulse length, in this case, an evaluation at 2 and 10 s, correlates more than 0.995 in all operating conditions except the charge pulse resistance at 80% SoC. At an aged condition, charge pulses will approach the upper cell voltage limit faster. Nevertheless, the correlation still is around 0.99 and it can be assumed that differences in pulse lengths are minimal and, therefore, different pulse lengths can be used for a comparison of aging trends. The highest and lowest current rates do not correlate as well. One explanation is that the voltage response for low current rates is also smaller, leading to a lower signal-to-noise ratio. In addition, high currents excite different chemical and physical processes, which can develop differently over the lifetime. The SoC levels compared in this dataset set at

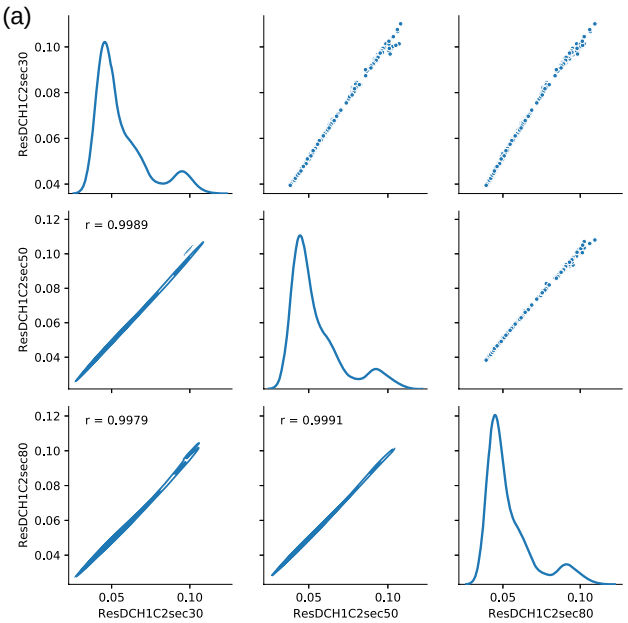

Scatterplot of 3 pulse resistance values of Baumhöfer dataset over all check-ups with the addition of the correlation coefficient of each pairing.

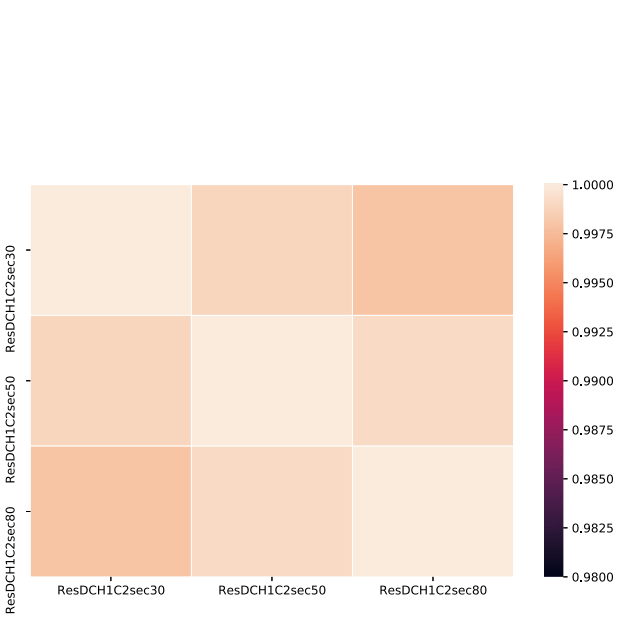

Heatmap of the same 3 pulse resistances as in Figure 4a of Baumhöfer dataset over all check-ups with the correlation coefficient as the color of the heatmap.

Figure 4. How to read the heat map.

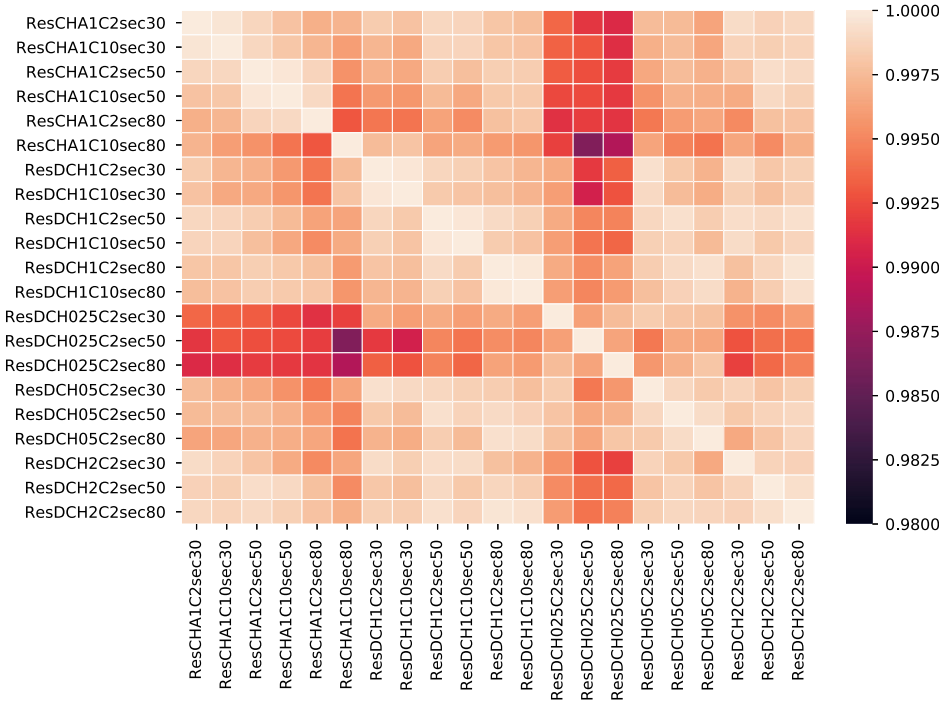

Figure 5. Heatmap of correlation of different pulse resistances of 30%, 50%, and 80% of Baumhöfer–2014 dataset. The color of the heatmap shows the correlation coefficient of each pairing in the matrix.

30%, 50%, and 80% highly correlate. To analyze the aging trend while limiting the time of a checkup procedure, one of these charge levels would give similar conclusions to three charge levels. But it can also be sensible for a more detailed analysis to include other SoCs since resistance also has an SoC dependence, especially at low and high SoCs.[24] In addition to pulse

resistances at defined SoCs, other resistances can be calculated without any additional measurements. Each current, either charge or discharge, generates a voltage change to determine a resistance value. For example, the first 10 s of a discharge can be handled as a pulse. Or, as Rumberg et al.[25] suggest, the resistance can be calculated after a discharge, with the last cell voltage measurement during discharge and the voltage the cell relaxes to. These values are without increased cost and have an additional benefit of tracking changes at the extremes of the voltage curve.

6. Test Condition Influence

Figure 6 shows the influence of different test conditions on the correlation of health indicators. For these three values, the discharge CapDCH1 capacity, the Ah throughput during constant current charge CAPCCCHA1, and one pulse resistance value were used. The test conditions all used a current of 1 C but were cycled with different cycle depths and mean SoC and with one cell each. The upper and lower SoC during cycling is shown in the legend. While the discharge and charge capacity show a strong correlation, slight differences are already visible for the different test conditions. When substituting health indicators for ones that are easy to measure, the relation must be independent of the history of prior cycling. This, unfortunately, cannot be observed, showing different resistance to capacity relations depending on the cycling condition. For higher cycling depths, capacity degrades quicker compared to the resistances in this dataset. Discharge and charge capacity show a high correlation and can likely be substituted for an aging analysis if one is not available. For the resistance capacity correlation, this is not the case, with clear differences visible for the different test conditions. For example, cycling from 0–100% shows the highest degradation of capacity in relation to the resistance measured. At around 35 Ah remaining discharge capacity, the pulse resistance is still below 2 mΩ, while cells from other test conditions already show a pulse resistance of up to 4 mΩ. When the aging condition triggers different aging regimes, the correlation will not be the same for those conditions. Similar results for different aging conditions but less pronounced are reported by Schuster et al.[26].

In addition to cycle tests, calendar-aged cells with a path dependency of the correlation are shown in **Figure 7**. Three cells were tested for each test condition and aged at 40 °C, except for one test at 25 °C and one at 60 °C, both at 66% SoC. At 40 °C, eight different SoCs were tested, ranging from 10% to 100%.

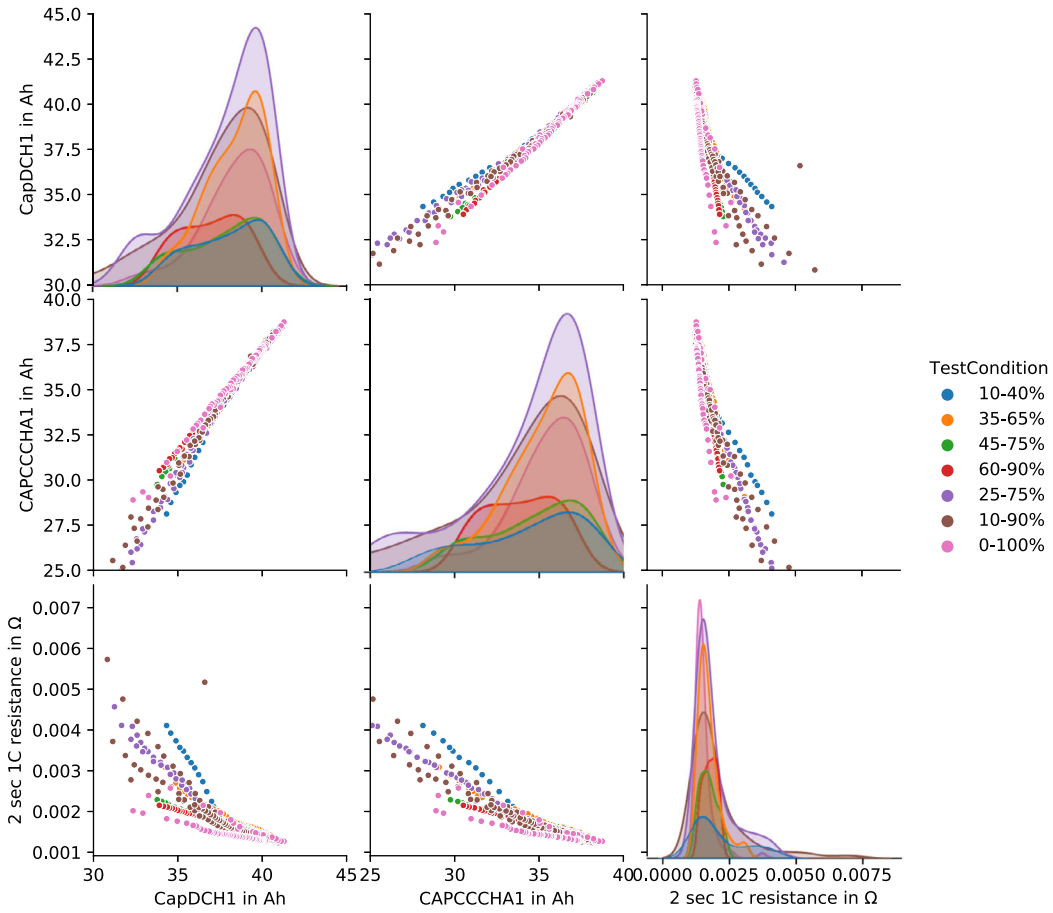

Figure 6. Correlation of discharge capacity, charge capacity, and pulse resistance over cycle aging for dataset Schöneberger–2019. Color represents different test conditions of cycle test with lower and upper SoC during cycling shown in the legend. The upper and lower triangles show the same data points.

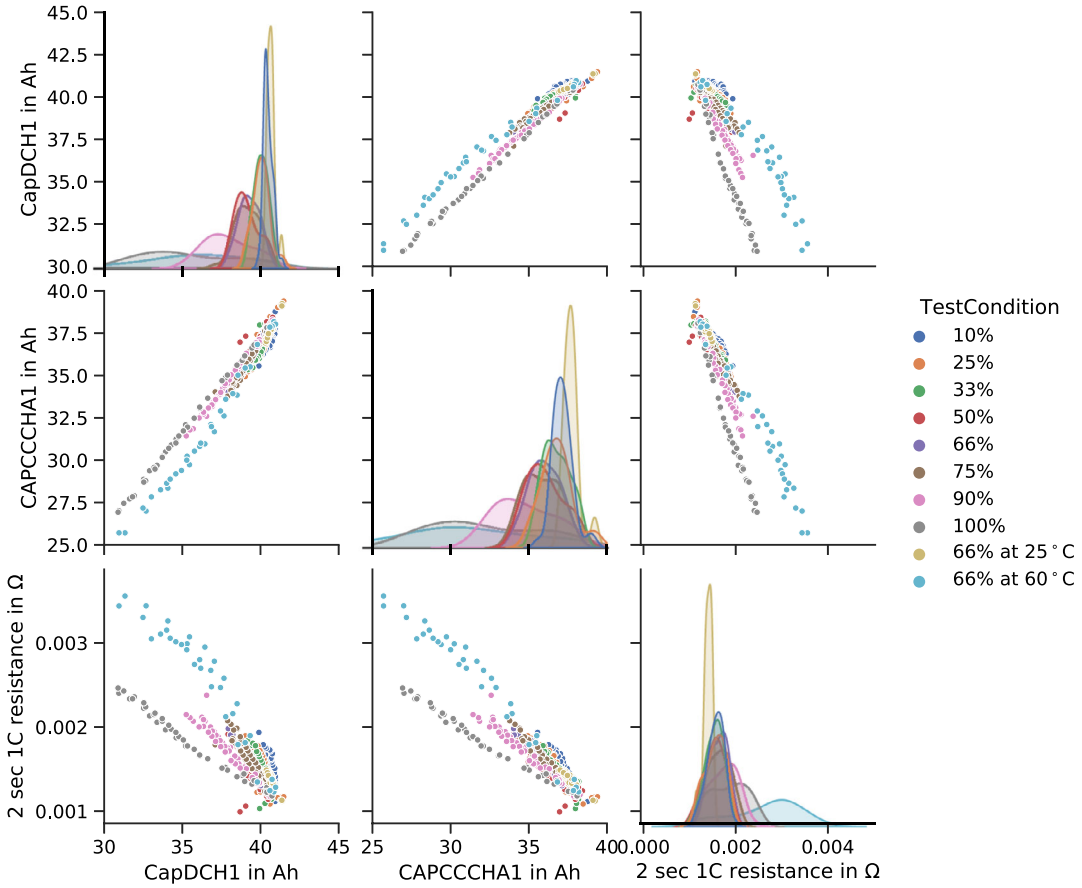

Figure 7. Correlation of discharge capacity, charge capacity, and pulse resistance over calendar aging for dataset Schönberger–2019. Color represents different test conditions of calendar test with SoC shown in the legend. The temperature of the test is 35 °C if not stated otherwise in legend. The upper and lower triangles show the same data points.

Just as the cycle-aged cell three values, the discharge CapDCH1 capacity, the Ah throughput during constant current charge CAPCCCHA1, and one pulse resistance value were used in the comparison. Similar to cycle aging, both capacity values strongly correlate with the 60 °C cells standing out, showing generally lower constant current charge capacities at similar discharge capacity levels. For cells at 60 °C, a disproportional increase of resistance can be seen. The highest SoC levels, 90% and 100%, also have higher capacity loss relative to the resistance increase.

7. Chemistry Influence

Figure 8 is based on the open dataset from Preger et al.[19] where three types of cells with different cathode chemistry are compared. In this set, the temperature for checkup procedures was kept at the same level as the cycling temperature. Since there is an influence of temperature on capacity and resistance, only cells cycled at 25 °C are considered. Each checkup procedure consists of three constant current constant voltage charges with 0.5 C up to the end of charge voltage and a discharge with 0.5 C. The correlation shows the discharge capacity values, the ampere-hours during the constant current phase of the first cycle, the ampere-hours during the constant voltage phase of the first cycle, the mean temperature during the first cycle, and a resistance value. The resistance is calculated with the difference of the relaxed voltage and 10 s into the discharge phase of the first cycle. Overall, the discharge capacity from the three cycles shows a high correlation, with less information with additional reference cycles.

8. Conclusion

Additional health indicators can be used to better understand a battery's state of health and define batteries as they age. In this study, we demonstrate the advantages of methodically examining numerous relationships among the primary health indicators. Other health markers also show cell-to-cell variance, in addition to capacity values, which are frequently illustrated in literature. Additionally, cell-to-cell variation shown in capacity values can exhibit strong correlations with other indicators' cell-to-cell variation while also displaying aging path-dependent correlation behavior. A comparison between the original cell-to-cell variance and aging tests was also made. Correlations for several cell types (cylindrical, pouch) and chemistries are included in this paper. But even so, the availability of the data constrained this research,

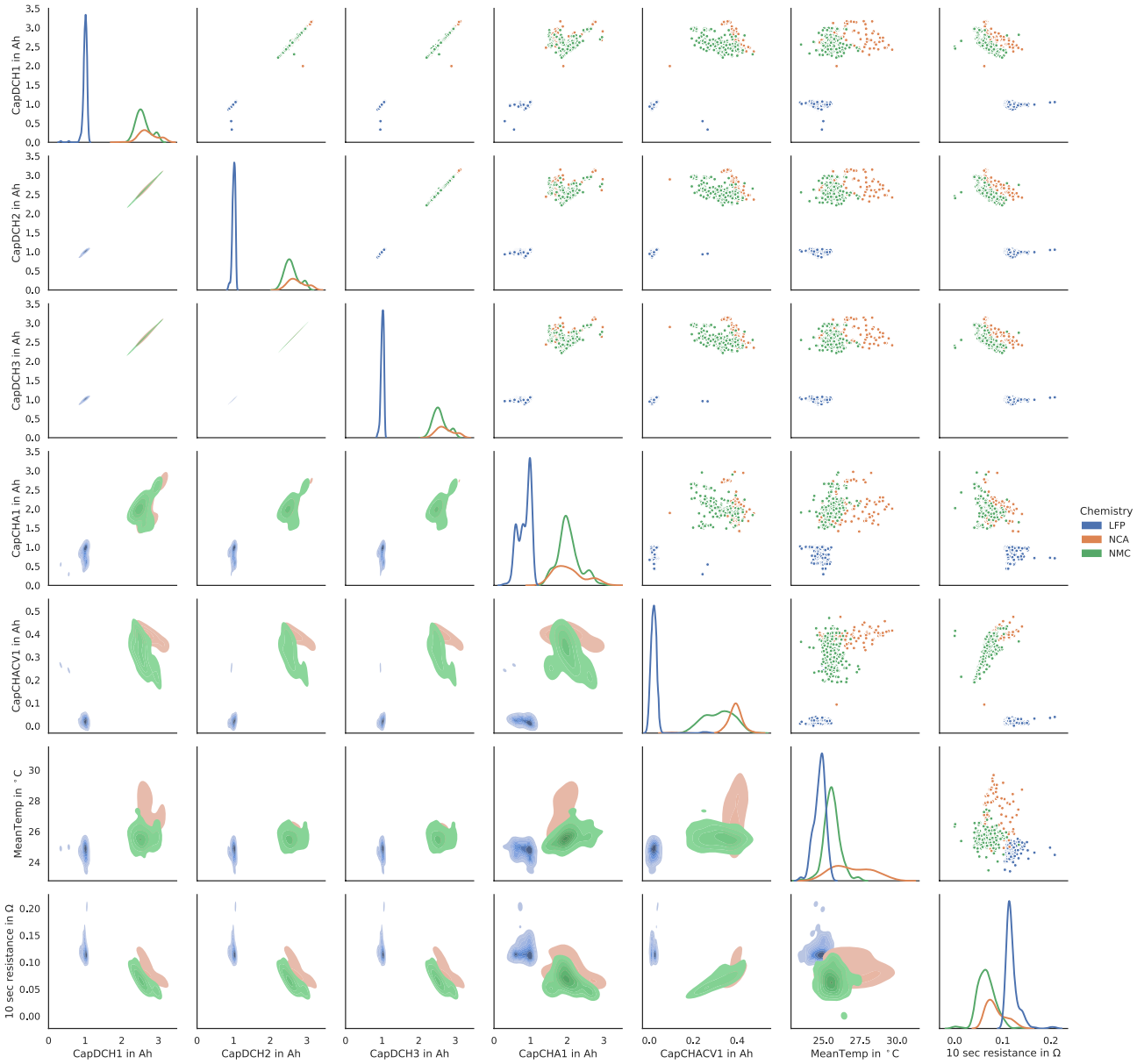

Figure 8. Comparison of correlation of NMC, NCA, and LFP of data from Preger et al. batteryarchive.org.

and it should be repeated as soon as sizable open-source datasets are made available to further our understanding of, say, variations in cell chemistries or form factors. Understanding the correlations of various health indicators can enable additional acceptable highly correlated metrics if performing reference performance tests is not practicable. Additionally, "free" measurements can be utilized to improve the accuracy of battery diagnostics. One example is the computation of resistance from an existing voltage drop in a battery management system. Although single-cell testing was the main emphasis of this article, modules or packs can also profit from understanding the correlation of health indicators, particularly in cases where the structure of the pack forbids single-cell measurements.

Acknowledgements

The authors would like to thank Thorsten Baumhöfer, Ilka Schöneberger, and Lisa Willenberg for generating the relevant datasets at the institute. Moreover, the possibility of an openly available dataset by Yuliya Preger et al. was highly appreciated. P.D. gratefully acknowledges the financial support by Bundesministerium für Bildung und Forschung (Grant no. BMBF 03XP0320A).

Open Access funding enabled and organized by Projekt DEAL.

Conflict of Interest

The authors declare no conflict of interest.

Author Contributions

P.D.: conceptualization, software, data curation, writing – original draft, visualization. E.B.: software, visualization. A.E. software, data curation. D.J: methodology, writing – review and editing. W.L.: methodology, writing – review and editing. D.U.S.: supervision, funding acquisition. S.L.: conceptualization, methodology, writing – original draft.

Data Availability Statement

The data that support the findings of this study are available from the corresponding author upon reasonable request.

Keywords

aging, batteries, capacity distribution, cell-to-cell variation, data mining, health indicators, lithium ion

Received: November 29, 2022
Revised: January 23, 2023
Published online:

[1] M. Dubarry, A. Devie, K. Stein, M. Tun, M. Matsuura, R. Rocheleau, *J. Power Sources* **2017**, *338*, 65.
[2] K. Rumpf, A. Rheinfeld, M. Schindler, J. Keil, T. Schua, A. Jossen, *J. Electrochem. Soc.* **2018**, *165*, A2587.
[3] H. Zappen, F. Ringbeck, D. U. Sauer, *Batteries* **2018**, *4*, 64.
[4] S. Rothgang, M. Rogge, J. Becker, D. U. Sauer, *Energies* **2015**, *8*, 6715.
[5] X-G. Yang, T. Liu, C-Y. Wang, *Nat. Energy* **2021**, *6*, 176.
[6] M. Wünsch, J. Kaufman, D. U. Sauer, *J. Energy Storage* **2019**, *21*, 149.
[7] D. Werner, S. Paarmann, A. Wiebelt, T. Wetzel, *Batteries* **2020**, *6*, 12.
[8] S. Müller, J. Eller, M. Ebner, C. Burns, J. Dahn, V. Wood, *J. Electrochem. Soc.* **2018**, *165*, A339.
[9] T. Baumhöfer, M. Brühl, S. Rothgang, D. U. Sauer, *J. Power Sources* **2014**, *247*, 332.
[10] N. H. Paulson, J. Kubal, L. Ward, S. Saxena, W. Lu, S. J. Babinec, *J. Power Sources* **2022**, *527*, 231127.
[11] P. K. Jones, U. Stimming, A. A. Lee, *Nat. Commun.* **2022**, *13*, 4806.
[12] M. Ecker, N. Nieto, S. Käbitz, J. Schmalstieg, H. Blanke, A. Warnecke, D. U. Sauer, *J. Power Sources* **2014**, *248*, 839.
[13] J. Schmalstieg, S. Käbitz, M. Ecker, D. U. Sauer, *J. Power Sources* **2014**, *257*, 325.
[14] J. Vetter, P. Novák, M.R. Wagner, C. Veit, K.-C. Möller, J.O. Besenhard, M. Winter, M. Wohlfahrt-Mehrens, C. Vogler, A. Hammouche, *J. Power Sources* **2005**, *147*, 269.
[15] M. Broussely, P. Biensan, F. Bonhomme, P. Blanchard, S. Herreyre, K. Nechev, R.J. Staniewicz, *J. Power Sources* **2005**, *146*, 90.
[16] D. Beck, P. Dechent, M. Junker, D. U. Sauer, M. Dubarry, *Energies*, **2021**, *14*, 3276.
[17] R. Li, J-F. Wu, H-Y. Wang, J-Y. Guo, Ge-C. Li, *Inform. Sci.* **2014**, *259*, 359.
[18] S. F. Schuster, M. J. Brand, P. Berg, M. Gleissenberger, A. Jossen, *J. Power Sources* **2015**, *297*, 242.
[19] Y. Preger, H. M. Barkholtz, A. Fresquez, D. L. Campbell, B. W. Juba, J. Romàn-Kustas, S. R. Ferreira, B. Chalamala, *J. Electrochem. Soc.* **2020**, *167*, 120532.
[20] I. Schoeneberger, P. Dechent, F. Rücker, S. Jakobowski, D. U. Sauer. *ECS Meet. Abstr.* **2019**, *MA2019-04*, 104.
[21] L. Willenberg, P. Dechent, G. Fuchs, M. Teuber, M. Eckert, M. Graff, N. Kürten, D. U. Sauer, E. Figgemeier, *J. Electrochem. Soc.* **2020**, *167*, 120502.
[22] M. Schindler, J. Sturm, S. Ludwig, J. Schmitt, A. Jossen, *eTransport.* **2021**, 100102.
[23] P. Kuntz, O. Raccurt, P. Azaïs, K. Richter, T. Waldmann, M. Wohlfahrt-Mehrens, M. Bardet, A. Buzlukov, S. Genies, *Batteries* **2021**, *7*, 48.
[24] P. S. Sabet, G. Stahl, D. U. Sauer, *J. Power Sources*, **2020**, *472*, 228189.
[25] B. Rumberg, K. Schwarzkopf, B. Epding, I. Stradtmann, A. Kwade, *J. Energy Storage* **2019**, *22*, 336.
[26] S. F. Schuster, M. J. Brand, C. Campestrini, M. Gleissenberger, A. Jossen, *J. Power Sources* **2016**, *305*, 191.